Journal of Biomolecular NMR **28:** 117–130, 2004.
KLUWER/ESCOM

GFT NMR experiments for polypeptide backbone and $^{13}C^{\beta}$ chemical shift assignment

Seho Kim[a,b,*] & Thomas Szyperski[a,b,**]
[a]*Department of Chemistry, University at Buffalo, The State University of New York, Buffalo, NY 14260, U.S.A.;*
[b]*The Northeast Structural Genomics Consortium*

Received 15 April 2003; Accepted 1 August 2003

Key words: automated protein NMR assignment, GFT NMR spectroscopy, high throughput, protein structure, structural genomics

Abstract

(4,3)D, (5,3)D and (5,2)D GFT triple resonance NMR experiments are presented for polypeptide backbone and $^{13}C^{\beta}$ resonance assignment of $^{15}N/^{13}C$ labeled proteins. The joint sampling of m = 2, 3 or 4 indirect chemical shift evolution periods of 4D and 5D NMR experiments yields the measurement of $2^m - 1$ linear combinations of shifts. To obtain sequential assignments, these are matched in corresponding experiments delineating either intra or interresidue correlations. Hence, an increased set of matches is registered when compared to conventional approaches, and the 4D or 5D information allows one to efficiently break chemical shift degeneracy. Moreover, comparison of single-quantum chemical shifts obtained after a least squares fit using either the intra or the interresidue data demonstrates that GFT NMR warrants highly accurate shift measurements. The new features of GFT NMR based resonance assignment strategies promise to be of particular value for establishing automated protocols.

Introduction

Recently introduced GFT NMR spectroscopy (Kim and Szyperski, 2003) provides high- dimensional spectral information with both accuracy and speed. The phase-sensitive joint sampling of several indirect dimensions of a high-dimensional NMR experiment leads to largely reduced minimum measurement times when compared to FT NMR. This allows one to avoid the 'sampling limited' data collection regime (Szyperski et al., 2002). Concomitantly, the analysis of the resulting chemical shift multiplets, which are edited by the G-matrix transformation, yields increased accuracy for the measurement of the chemical shifts. To indicate that a combined G-matrix and Fourier transformation (FT) is employed, the approach was named 'GFT' NMR spectroscopy (Kim and Szyperski, 2003).

GFT NMR spectroscopy is derived from 'modules' that were developed in the 1990s, triggered by the invention of two-spin coherence spectroscopy (Szyperski et al., 1993a) and its generalization, reduced-dimensionality (RD) NMR spectroscopy (Szyperski et al., 1993b). Two-spin coherence spectroscopy has also been named MQ (Simorre et al., 1994) or ZQ/DQ NMR spectroscopy (Rexroth et al., 1995), and was employed for measuring scalar couplings (Rexroth et al., 1995), dipole-dipole (Reif and Hennig, 1997) and dipole-CSA cross-correlated relaxation (e.g., Brutscher et al., 1998). It has been suggested (Ding and Gronenborn, 2002; Bersch et al., 2003) that RD NMR represents a variant of 'accordion spectroscopy' (Bodenhausen and Ernst, 1982), which was previously designed to jointly sample a chemical shift evolution and the mixing time employed in exchange spectroscopy (EXSY). However, the time evolution of longitudinal magnetization during the mixing time in EXSY (or NOESY) differs from the jointly incremented chemical shift time evolution in RD NMR. Thus, the two approaches lack similarity in terms of

*Current address: Department of Chemistry, Rutgers University, Piscataway, NJ 08854, U.S.A.
**To whom correspondence should be addressed. E-mail: szypersk@chem.buffalo.edu

(i) implementation of data acquisition, (ii) observed peak pattern and (iii) registered line shapes, and it is tempting to propose that RD NMR and accordion spectroscopy represent distinct NMR spectroscopic concepts.

RD NMR was complemented by (i) the relative scaling of the two jointly sampled indirect evolution times, as proposed by Szyperski et al. (1993b) and implemented by Brutscher et al. (1994) and Szyperski et al. (1994), and (ii) the use of time proportional phase incrementation (TPPI) to position the carrier of the projected dimension at the edge of the spectral range (Brutscher et al., 1995a). In an ingenious fashion, Brutscher et al. (1995b) have then introduced the phase sensitive joint sampling of two chemical shifts, an approach that could be named 'edited phase sensitive' RD NMR, since the two peaks forming the RD NMR peak pair can be separated into two subspectra. Moreover, it was shown that the symmetrization of RD NMR spectra allows one to recover the sensitivity (Brutscher et al., 1995a) and the dispersion of the higher- dimensional parent experiment (Szyperski et al., 1995). A pivotal step toward preserving the full potentialities of the parent experiment was the detection of peaks defining the center of the RD NMR peak pairs. This can be achieved either by incomplete INEPT (Szyperski et al., 1995) or using ^{13}C steady state magnetization (Szyperski et al., 1996). Notably, the latter RD NMR experiments were the first multidimensional NMR experiments recruiting the magnetization of both ^{1}H and heteronuclei for signal detection. To circumvent spectral editing, combined scaling of shift evolution periods and TPPI was employed to place central peaks and components of the peak pairs into distinct spectral regions (Szyperski et al., 1995, 1998). Recently, the particular demands of structural genomics (Montelione et al., 2000) lead to the employment of RD NMR for high throughput (HTP) structure determination (Szyperski et al., 2002), and Xia et al. (2002) proposed to use RD NMR in conjunction with simultaneous NMR data acquisition (e.g., Boelens et al., 1994). In another vein, Löhr and Rüterjans (1995) introduced the two-fold application of the RD NMR approach, in which the transfer amplitude is cosine modulated twice with the chemical shifts of two different nuclei. This leads to a two-fold reduction of the dimensionality, and Ding and Gronenborn (2002) have recently introduced valuable new 'double RD NMR' experiments. Very recently, Bersch et al. (2003) nicely demonstrated the use of edited phase sensitive RD NMR for measuring residual dipolar couplings (for a recent review, see Bax, 2003), which allows one to potentially recruit such couplings to support the sequential resonance assignment (Zweckstetter and Bax, 2001). Shortly after the GFT NMR formalism (Kim and Szyperski, 2003) was published on-line, Kozminski and Zhukov (2003) submitted a paper describing a double phase sensitively detected RD NMR experiment corresponding to the basic spectra of a (4,2)D GFT NMR experiment. For the sake of completeness, it shall be mentioned here that RD NMR has been employed for assigning polypeptide backbone (Astrof et al., 2001) and side-chain chemical shifts (Luca and Baldus, 2002) in solid state NMR spectroscopy, as well as for studying nucleic acids (e.g., Sklenar et al., 1998).

GFT NMR spectroscopy (Kim and Szyperski, 2003) combines (i) multiple phase sensitive RD NMR, (ii) multiple 'bottom-up' central peak detection, and (iii) (time domain) editing of the components of the chemical shift multiplets. The resulting formalism embodies a flexible, generally applicable NMR data acquisition scheme. Provided that $m = K + 1$ chemical shift evolution periods of an ND experiments are jointly sampled in a single indirect 'GFT dimension', $p = 2^m - 1$ different (N-K)D spectra represent the GFT NMR experiment containing the information of the parent ND experiment. Hence, such a set of p spectra was named an (N,N-K)D GFT NMR experiment (Kim and Szyperski, 2003). In this publication we present a suite of (4,3)D, (5,3)D and (5,2)D ^{13}C/^{15}N/^{1}H triple resonance GFT NMR experiments for the assignment of polypeptide backbone and $^{13}C^{\beta}$ chemical shifts, including a new pulse scheme to acquire (4,3)D CBCA,CONHN.

Methods

The following GFT NMR experiments were implemented (Figure 1): (i) with $K = 3$, (5,2)D HACA,CONHN complementing previously published (5,2)D HACACONHN (Kim & Szyperski, 2003) for sequential assignment, (ii) with $K = 2$, (5,3)D HACA,CONHN and (5,3)D HACACONHN, where in contrast to the (5,2)D experiments in (i) we have that the ^{15}N chemical shifts evolve separately, and (iii) with $K = 1$, (4,3)D CBCACONHN and (4,3)D CBCA,CONHN. The underlined letters indicate which chemical shifts that are jointly sampled. After G-matrix transformation one obtains $2^{K+1} - 1 = 15$ 2D planes for the (5,2)D exper-

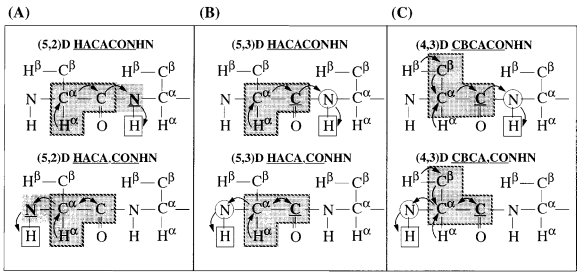

Figure 1. Magnetization transfer pathways of GFT NMR experiments. (A) (5,2)D HACACONHN and (5,2)D HACA,CONHN, (B) (5,3)D HACACONHN and (5,3)D HACA,CONHN, and (C) (4,3)D CBCACONHN and (4,3)D CBCA,CONHN. INEPT-type polarization transfers (Cavanagh et al., 1996) are indicated by arrows, and Löhr's 'en passant' frequency labeling module (see text) is indicated by a double arrow. The nuclei for which the chemical shift is detected in quadrature are shown in bold and are underlined. The nuclei with a grey background are simultaneously sampled in the GFT NMR dimension, and the chemical shifts of the boxed nuclei are used to establish sequential connectivities. In (B), the chemical shifts of nitrogen spins shown in circles are measured is a separate dimension.

iments (K = 3), seven 3D spectra for the (5,3)D experiments (K = 2) and three 3D spectra for the (4,3)D experiments (K = 1). The magnetization transfer pathways are depicted in Figure 1. Spectra were acquired for the 8.6 kDa protein ubiquitin and for the 14 kDa protein TT212 from the protein structure production pipeline of the Northeast Structural Genomics Consortium (http://www.nesg.org).

(5,2)D HACA,CONHN / (5,2)D HACACONHN and (5,3)D HACA,CONHN / (5,3)D HACACONHN correlate the backbone amide ^{15}N and ^{1}H^{N} chemical shifts of residue i with the ^{13}C′, ^{13}C$^{\alpha}$ and ^{1}H$^{\alpha}$ chemical shifts of residue i − 1 and i, respectively, via one-bond scalar couplings (Figures 1A, B). In addition, the often smaller two-bond scalar couplings between the ^{15}N$_{i}$ and ^{13}C$^{\alpha}$ i − 1 may yield sequential connectivities in the HACA,CONHN experiments. The comma separating 'CA' from 'CO' indicates that the intraresidue ^{13}C′ chemical shift is obtained by creating two-spin coherence involving ^{13}C$^{\alpha}$ and ^{13}C′ during the intraresidue polarization transfer from ^{13}C$^{\alpha}$ to ^{15}N (Löhr and Rüterjans, 1995).

The (5,2)D HACA,CONHN experiment was recorded with the radio-frequency (r.f.) pulse scheme of Figure 2A, and we refer to Löhr and Rüterjans (1995) for a product operator description of the experiment. Since r.f. pulses on ^{13}C′ are employed as laminar shifted pulses (Cavanagh et al., 1996), the spectral width of the indirect dimension was set to one half of the difference of the ^{13}C$^{\alpha}$ and ^{13}C′ carrier frequencies (8,897 Hz at 600 MHz) in order to fold the ^{13}C′ onto the ^{13}C$^{\alpha}$ carrier frequency. In the current implementation of (5,2)D HACA,CONHN, $\Omega(^{15}N)$ was detected in quadrature in the GFT dimension ω_1. With the GFT NMR super phase-cycle given in the legend of Figure 2A, this yields (i) eight basic 2D spectra with peaks at $\Omega_0(^{15}N)\pm\Omega_1(^{13}C')\pm\Omega_2(^{13}C^{\alpha})\pm\Omega_3(^{1}H^{\alpha})$ along ω_1, (ii) four 2D first order central peak spectra with peaks at $\Omega_0(^{15}N)\pm\Omega_1(^{13}C')\pm\Omega_2(^{13}C^{\alpha})$, (iii) two 2D second order central peak spectra with peaks at $\Omega_0(^{15}N)\pm\Omega_1(^{13}C')$ and (iv) one 2D third order central peak spectrum with peaks at $\Omega_0(^{15}N)$. The choice for the order of central peak detection is primarily guided by sensitivity considerations. First order central peaks were derived from ^{13}C$^{\alpha}$ magnetization as described (Kim and Szyperski, 2003), which allows one to detect these central peaks while the basic spectra are acquired. Hence, when the basic spectra are acquired with at least two scans per increment, the first order central peaks are obtained from ^{13}C steady state magnetization without investment of additional measurement time. In case single scan acquisition is chosen for the basic spectra, first order central peak detection would be best implemented by simply omitting the ^{1}H$^{\alpha}$ shift evolution. Second order central peak were derived from ^{1}H$^{\alpha}$ magnetization using the scheme of Figure 2A, i.e., by omitting both the ^{1}H$^{\alpha}$ and ^{13}C$^{\alpha}$ chemical shift evolution periods. This approach is more sensitive than using 2D HNN(CA)CO. Finally, sensitive 2D [^{15}N,^{1}H]-HSQC provided the third order central peaks. To match (5,2)D HACA,CONHN, (5,2)D HACACONHN (Figure 1A) was acquired with the same order for central peak detection as described (Kim and Szyperski; 2003), except that the spectral width of the indirect GFT dimension was set to 8,897 Hz (see above).

(5,3)D HACACONHN and HACA,CONHN were recorded using the pulse scheme and a correspondingly reduced GFT NMR super phase cycle of the (5,2)D congeners (Figure 1A); $\Omega(^{13}C')$ was detected in quadrature in the GFT dimension and $\Omega(^{15}N)$ was sampled in a separate chemical shift evolution along ω_2. This yields (i) four basic 3D spectra with peaks at $\Omega_0(^{13}C')\pm\Omega_1(^{13}C^{\alpha})\pm\Omega_2(^{1}H^{\alpha})$, (ii) two first order central peak spectra with peaks at $\Omega_0(^{13}C')\pm\Omega_1(^{13}C^{\alpha})$ and (ii) one second order central peak spectrum with peaks at $\Omega_0(^{13}C')$.

(4,3)D CBCACONHN and (4,3)D CBCA,CONHN correlate the backbone amide ^{15}N and ^{1}HN chemical shifts of residue i with the ^{13}C', ^{13}C$^{\alpha}$ and ^{13}C$^{\beta}$ chemical shifts of residue i − 1 and i, respectively,

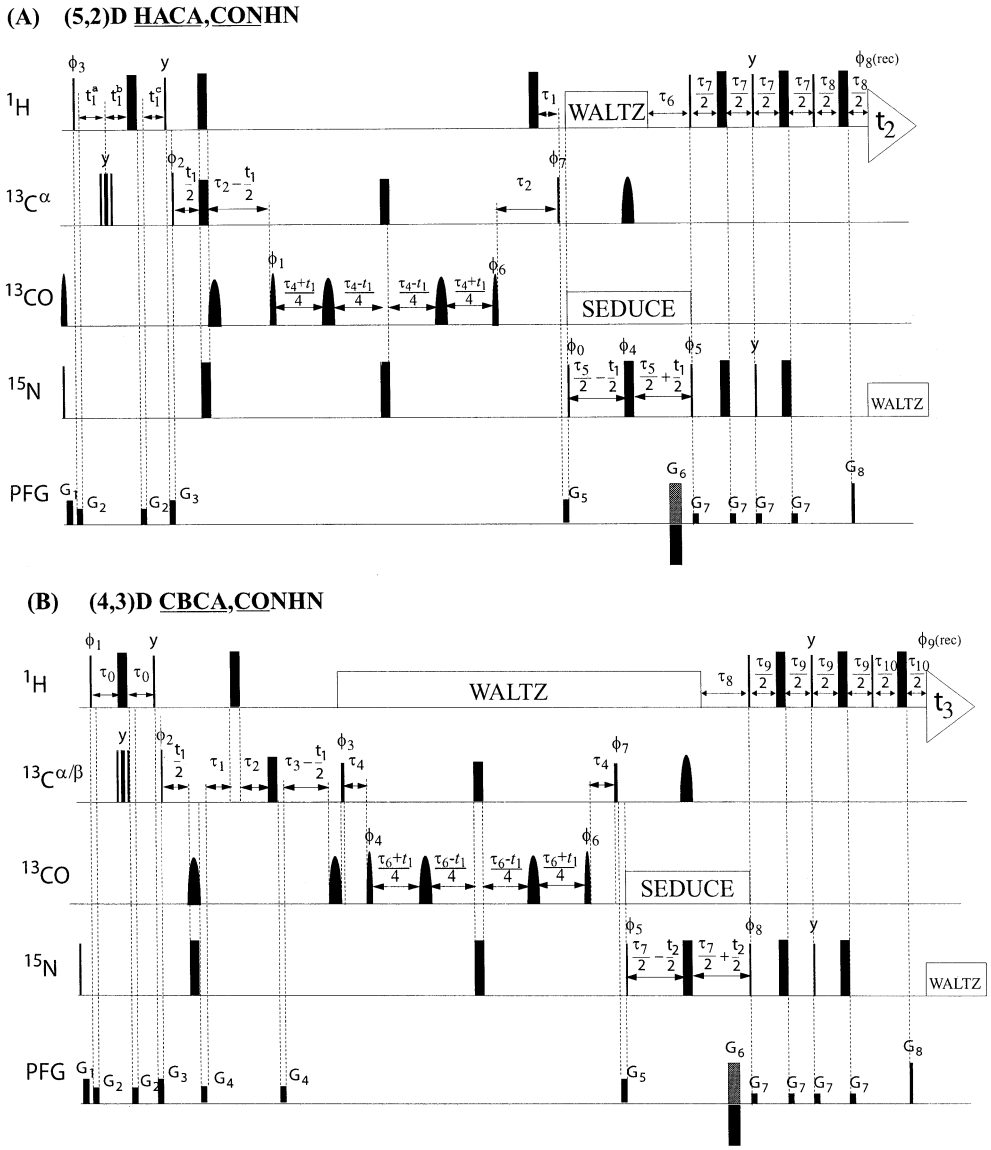

Figure 2. Experimental scheme for the (A) (5,2)D HACA,CONHN and (B) (4,3)D CBCA,CONHN GFT NMR experiments. Rectangular 90° and 180° pulses are indicated by filled and open vertical bars or shaped pulses, respectively, and phases are indicated above the pulses. Where no radio-frequency (r.f.) phase is marked, the pulse is applied along x. The high power 90° pulse lengths were: 5.8 μs for ^{1}H and 15.4 μs for ^{13}C, and 38 μs for ^{15}N. In (A), pulses on ^{13}C prior to t_1(^{13}C) are applied at high power, and ^{13}C decoupling during t_1(^{1}H) is achieved using a (90_x-180_y-90_x) composite pulse (Cavanagh et al., 1996). Subsequently, the 90° and 180° pulse lengths of $^{13}C^{\alpha}$ are adjusted to 51.5 μs and 46 μs, respectively, to minimize perturbation of the ^{13}CO spins. The width of the 90° pulses applied to ^{13}CO pulse is 52 μs and the corresponding 180° pulses are applied with same power. A SEDUCE (Cavanagh et al., 1996) 180° pulse with a length 252 μs is used to decouple ^{13}CO during t_1(^{13}C). WALTZ16 (Cavanagh et al., 1996) is employed to decouple ^{1}H (r.f. field strength = 9.2 kHz) during the heteronuclear magnetization transfers as well as to decouple ^{15}N (r.f. = 1.78 kHz) during acquisition. The SEDUCE sequence (r.f. = 1.0 kHz) is used for decoupling of $^{13}C^{\alpha}$ during the ^{15}N chemical shift evolution period. The ^{1}H r.f. carrier is placed at 4.78 ppm. The $^{13}C^{\alpha}$ and ^{15}N r.f. carriers are set to 56.3 ppm and 119.3 ppm, respectively. All $^{13}C'$ pulses are laminar shifted (Cavanagh et al., 1996) by 118 ppm relative to the $^{13}C^{\alpha}$ carrier position. By setting the spectral width of the jointly sampled dimension to one half of 118 ppm, the apparent carrier position for sampling of $^{13}C'$ chemical shift (174.3 ppm) is folded on the position of the $^{13}C^{\alpha}$ carrier position at 56.3 ppm. The duration and strengths of the pulsed z-field gradients (PFGs) are: G_1 (1 ms, 24 G/cm); G_2 (100 μs, 16 G/cm); G_3 (1 ms, 24 G/cm); G_5 (1.5 ms, 20 G/cm); G_6 (1.25 ms, 30 G/cm); G_7 (500 μs, 8 G/cm); G_8 (125 μs, 29.5 G/cm). All PFG pulses are of rectangular shape. The delays are: $\tau_1 = 1.6$ ms, $\tau_2 = 9.0$ ms, $\tau_4 = 11.0$ ms, $\tau_5 = 22.0$ ms, $\tau_6 = 5.5$ ms, $\tau_7 = 4.6$ ms, $\tau_8 = 1$ ms. ^{1}H-frequency labeling is achieved in a semi constant-time fashion with $t_1{}^a$ (0) = 1.7 ms, $t_1{}^b$ (0) = 1 μs, $t_1{}^c$ (0) = 1.701 ms, $\Delta t_1{}^a = 60$ μs, $\Delta t_1{}^b = 35.4$ μs, $\Delta t_1{}^c = -24.6$ μs. Hence, the fractional increase of the semi constant-time period with t_1 equals to $\lambda = 1 + \Delta t_1{}^c / \Delta t_1{}^a = 0.58$. Phase cycling for artefact suppression: $\phi_0 = x$; $\phi_1 = x, -x$; $\phi_2 = x, x, -x, -x$; $\phi_3 = x$;

Figure 2. ϕ_4 = 4x, 4(−x); ϕ_5 = x; $\phi_6 = \phi_7$ = x; ϕ_8(receiver) = 2(x,−x,−x,x). Phases ϕ_6 and ϕ_7 are shifted by 50° to compensate for non-resonance effects. GFT NMR super phase-cycling for recording the 8 basic spectra: ϕ_1 = x,y; ϕ_2 = 2x,2y; ϕ_3 = 4x,4y (the *G*-matrix required for time domain editing is shown in Equation S12 of the Supplementary information of Kim and Szyperski, 2003). For acquisition of central peaks derived from ^{13}C steady state magnetization, a second set of data sets with a 180° shift for ϕ_3 is collected and data are 'pre-processed' as described (see Equations S10 and S11 in the Supplementary information of Kim and Szyperski, 2003). For second order central peak detection, the ^{1}H$^\alpha$ and ^{13}C$^\alpha$ chemical shift evolution periods are omitted and ϕ_1 = x,y; ϕ_2 = x; ϕ_3 = x. Third order central peaks were detected in 2D [^{15}N,^{1}H]-HSQC (Cavanagh et al., 1996). (The *G*-matrices required for the central peak spectra are shown in Equations S13 to S15 of the Supplementary information of Kim and Szyperski, 2003). The sensitivity enhancement scheme of Kay et al. (1992) is employed, i.e., the sign of G6 is inverted in concert with a 180° shift of ϕ_5. For implementation of (5,3)D HACA,CONHN, t_1(^{15}N) is replaced by t_2(^{15}N), and quadrature detection in t_1 is accomplished by altering the phase ϕ_1 according to States-TPPI. GFT NMR super phase cycle for the 4 basic spectra: ϕ_2 = x,y; ϕ_3 = 2x,2y (the *G*-matrix required for time domain editing is shown in Equation S13 of the Supplementary information of Kim and Szyperski, 2003). First order central peaks are derived from ^{13}C magnetization and are obtained by acquiring a second set of data sets with a 180° shift for ϕ_3. For second order central peak detection, t_1(^{1}H$^\alpha$) and t_1(^{13}C$^\alpha$) is omitted. (The *G*-matrices required for time domain editing of the central peak spectra are shown in Equations S14 and S15 of the Supplementary information of Kim and Szyperski, 2003). In (B), pulses on ^{13}C prior to t_1(^{13}C) are applied at high power. Subsequently, the 90° and 180° pulse lengths applied for ^{13}C$^{\alpha/\beta}$ are adjusted to 47.5 μs and 42.5 μs, respectively, to minimize perturbation of ^{13}CO spins. The width of the 90° pulses applied to ^{13}CO pulse is 52 μs and the corresponding 180° pulses are applied with same power. SEDUCE 180° pulses of 200 μs pulse length are used to decouple ^{13}CO during t_1 and τ_4. WALTZ16 is employed to decouple ^{1}H (r.f. field strength = 9.2 kHz) during the heteronuclear magnetization transfers, as well as to decouple ^{15}N (r.f. = 1.78 kHz) during acquisition. The SEDUCE sequence is used for decoupling of ^{13}C′ during the ^{15}N chemical shift evolution period (r.f. = 1.0 kHz). The ^{1}H r.f. carrier is placed at 4.78 ppm. Initially, the ^{13}C′ and ^{15}N r.f. carriers are set to 41.3 ppm and 119.3 ppm, respectively. The ^{13}C′ carrier position is folded from 174.3 to 41.3 ppm by setting the spectral width in ω_1 to one half of 133 ppm (= 174.3 ppm − 41.3 ppm; see also text). The ^{13}C carrier is set to 56.3 ppm during the τ_7 delay. The duration and strengths of the pulsed z-field gradients (PFGs) are: G_1 (1 ms, 24 G/cm); G_2 (100 μs, 16 G/cm); G_3 (250 μs, 29.5 G/cm); G_4 (250 μs, 30 G/cm); G_5 (1.5 ms, 20 G/cm); G_6 (1.25 ms, 30 G/cm); G_7 (500 μs, 8 G/cm); G_8 (125 μs, 29.5 G/cm). All PFG pulses are of rectangular shape. The delays are: τ_0 = 1.7 ms, τ_1 = 800 μs, τ_2 = 2.8 ms, τ_3 = 3.3 ms, τ_4 = 6.6 ms, τ_6 = 8.8 ms, τ_7 = 24 ms, τ_8 = 5.5 ms, τ_9 = 4.6 ms, τ_{10} = 1.0 ms. Phase cycling for artefact suppression: $\phi_1 = x$; ϕ_2 = 2(x), 2(−x); ϕ_3 = x; ϕ_4 = x, −x; $\phi_5 = \phi_6 = \phi_7 = \phi_8$ = x; ϕ_9(receiver) = x,−x,−x,x. Phases ϕ_6 and ϕ_7 are shifted by 120° to compensate for non-resonance effects. GFT NMR super phase-cycling for recording the two basic spectra: ϕ_2 = x,y (the *G*-matrix required for time domain editing is shown in Equation S14 of the Supplementary information of Kim and Szyperski, 2003). The sensitivity enhancement scheme of Kay et al. (1992) is employed, i.e., the sign of G6 is inverted in concert with a 180° shift of ϕ_8. Quadrature detection in t_1(^{13}C′) is accomplished by altering the phase ϕ_6 according to States-TPPI (Cavanagh et al., 1996).

via one-bond scalar couplings (Figure 1C), and the often smaller two-bond scalar couplings between the ^{15}N$_i$ and ^{13}C$^\alpha$ i − 1 may yield additional sequential connectivities in (4,3)D CBCA,CONHN. Ω(^{13}C′) was detected in quadrature in the GFT dimension thus yielding (i) two basic 3D spectra with peaks at Ω_0(^{13}C′)±Ω_1(^{13}C$^\alpha$) and Ω_0(^{13}C′)±Ω_1(^{13}C$^\beta$) and (ii) one central peak spectrum with peaks at Ω_0(^{13}C′). (4,3)D CBCACONHN was recorded by modifying the H$^{\alpha/\beta}$C$^{\alpha/\beta}$(CO)NHN pulse scheme (derived from CBCA(CO)NHN; Grzesiek and Bax, 1992) described in Szyperski et al. (2002): The ^{1}H$^{\alpha/\beta}$ chemical shift evolution was eliminated and a ^{13}C′ chemical shift evolution was introduced in a constant-time manner (see Figure S1 of the Supplementary material to be obtained from the authors for the r.f. pulse scheme). (4,3)D CBCA,CONHN was recorded with the new pulse scheme shown in Figure 2B, that is, ^{13}C′-^{13}C$^\alpha$ two-spin coherence is created for simultaneous ^{13}C′ and ^{13}C$^\alpha$ frequency labeling during the polarization transfer from ^{13}C$^\alpha$ to ^{15}N.

Results and discussion

We acquired on a VARIAN Inova 600 MHz spectrometer at 25 °C: (i) (5,2)D HACACONHN (2.5 h measurement time), (5,2)D HACA,CONHN (8.1 h), (ii) (5,3)D HACACONHN (10.4 h) and (5,3)D HACA,CONHN (10.4 h) and (iii) (4,3)D CBCACONHN (5.6 h) and (4,3)D CBCA,CONHN (5.6 h) for a 2 mM solution (pH = 5.8, 50 mM K-PO_4, 90% H2O/10% D_2O) of the 8.6 kDa protein ubiquitin. (5,3)D HACACONHN (20.8 h) and (5,3)D HACA,CONHN (41.8 h) were also acquired for a 1 mM solution (pH = 6.5, 450 mM NaCl, 10 mM DTT, 20 mM Zn^{2+}, 0.01% NaN_3, 95% H_2O/5% D_2O) of the 14 kDa protein structural genomics target protein TT212.

The yield of peak detection, i.e. the ratio of observed peaks over the total number of expected peaks, was (virtually) complete throughout. Reductions in minimal measurement time, ε, achievable in GFT NMR are given by the ratio of the number of free induction decays (FIDs) of an (N,N-K)D GFT NMR experiment over and the number FIDs of the ND FT NMR experiment (Kim and Szyperski, 2003). (A) For ubiquitin we obtained: (i) (5,2)D HACACONHN

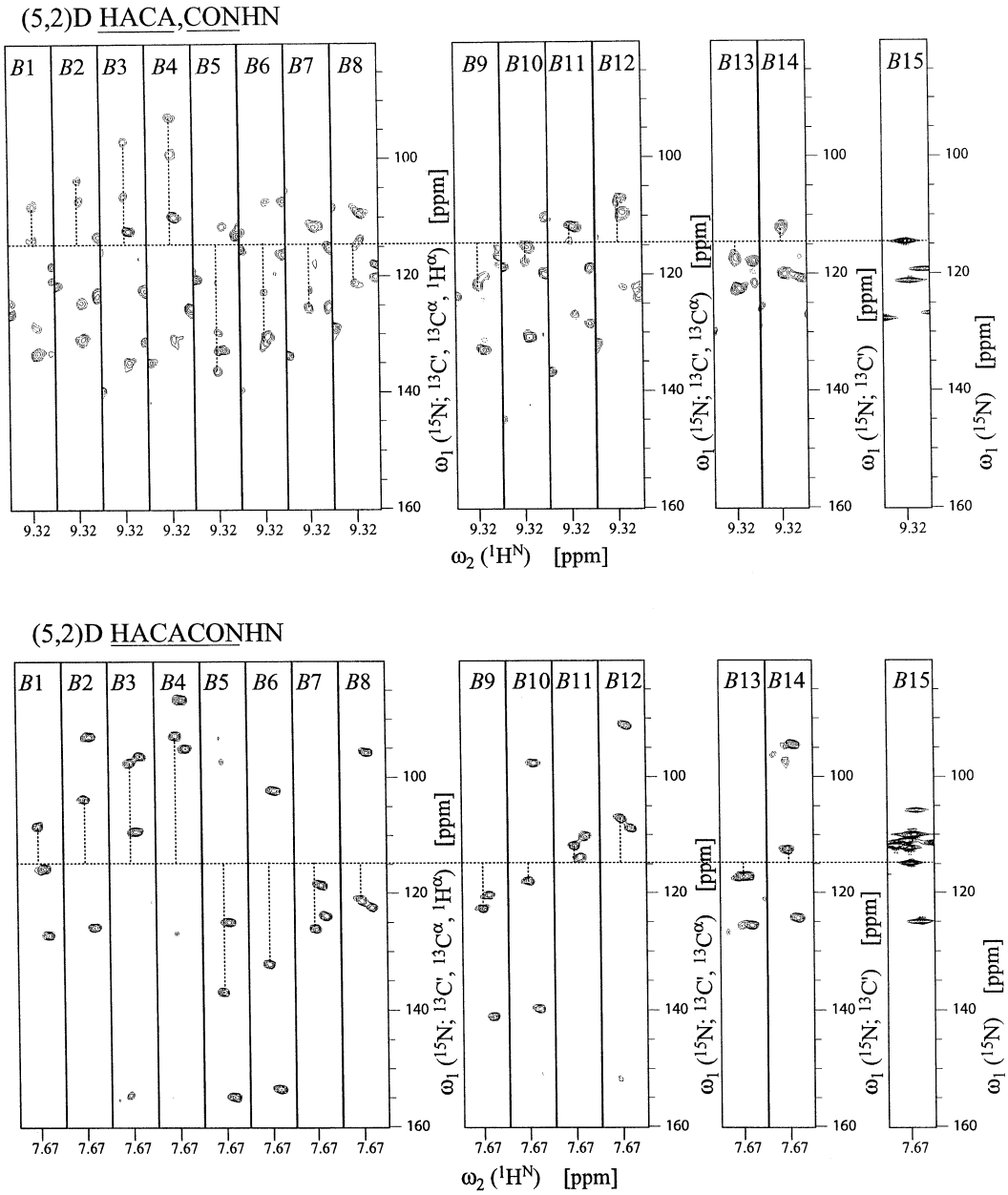

Figure 3. Composite plot of $[\omega_1,\omega_2]$-strips taken from (5,2)D HACA,CONHN (A) and HACACONHN data (B) collected for the 8.6 kDa protein ubiquitin with a total measurement time of 10.5 hours. The 2D data were acquired with $58(t_1) \times 512(t_2)$ complex points and $t_{1\,max}(^{15}N; {}^{13}C', {}^{13}C^{\alpha}, {}^{1}H^{\alpha}) = 6.5$ ms and $t_{2\,max}(^{1}H^{N}) = 73.2$ ms. In (A), the strips were taken from basic spectra (*B*1 to *B*8), first order central peak spectra (*B*9 to *B*12), second order central peak spectra (*B*13 and *B*14) and third order central peak spectra (*B*15) and are centered about the amide proton chemical shift of Glu 64. The position of the backbone ^{15}N chemical shift of Glu 64 is indicated by a dashed horizontal line, and the type of linear combination of chemical shifts detected for a given strip along ω_1 is indicated at the top of the strip: *B*1 $[\Omega_0+\Omega_1+\Omega_2+\Omega_3]$; *B*2 $[\Omega_0-\Omega_1+\Omega_2+\Omega_3]$; *B*3 $[\Omega_0+\Omega_1-\Omega_2+\Omega_3]$; *B*4 $[\Omega_0-\Omega_1-\Omega_2+\Omega_3]$; *B*5 $[\Omega_0+\Omega_1+\Omega_2-\Omega_3]$; *B*6 $[\Omega_0-\Omega_1+\Omega_2-\Omega_3]$; *B*7 $[\Omega_0+\Omega_1-\Omega_2-\Omega_3]$; *B*8 $[\Omega_0-\Omega_1-\Omega_2-\Omega_3]$; *B*9 $[\Omega_0+\Omega_1+\Omega_2]$; *B*10 $[\Omega_0-\Omega_1+\Omega_2]$; *B*11 $[\Omega_0+\Omega_1-\Omega_2]$; *B*12 $[\Omega_0-\Omega_1-\Omega_2]$; *B*13 $[\Omega_0+\Omega_1]$; *B*14 $[\Omega_0-\Omega_1]$; *B*15 $[\Omega_0]$. In (B), the corresponding strips are centered about the amide proton chemical shift of Ser 65. The variation of the 15 peaks relative to the ^{15}N chemical shift of Ser 65 (indicated by a dashed horizontal line) matches the variation about the ^{15}N chemical shift of Glu 64 in (A). This allows one to establish the sequential connectivity between Glu 64 and Ser 65 based on the measurement of three chemical shifts, i.e., $\Omega(^{13}C')$, $\Omega(^{13}C^{\alpha})$ and $\Omega(^{1}H^{\alpha})$. The shifts are obtained with high precision (Table 1) since the errors are reduced by the following factors when compared with FT NMR (calculated as described in Kim and Szyperski, 2003). For $\Omega(^{15}N)$: $\sqrt{15} = 3.9$; $\Omega(^{13}C')$: $\sqrt{14} = 3.7$; $\Omega(^{13}C^{\alpha})$: $\sqrt{12} = 3.5$; $\Omega(^{1}H^{\alpha})$: $\sqrt{8} = 2.8$. ^{1}H and ^{13}C chemical shifts are in ppm relative to 2,2-dimethyl-2-silapentane-5-sulfonate sodium salt (DSS).

($\varepsilon = 225$; 100% yield; S/N for peaks in basic spectra: 6.9–14.8; in first order central peak spectra: 8.1–10.4), (5,2)D HACA,CONHN ($\varepsilon = 225$; intraresidue correlations: 100% yield; S/N for peaks in basic spectra: 4.0–6.8; in first order central peak spectra: 3.3–5.3), (ii) (5,3)D HACACONHN ($\varepsilon = 25$; 100% yield; S/N for peaks in basic spectra: 27.5–61.2; in first order central peak spectra: 26.2–41.3) and (5,3)D HACA,CONHN ($\varepsilon = 25$; intraresidue correlations: 100% yield; S/N for peaks in basic spectra: 14.7–23.6; 93% in first order central peak spectra: 13.1–22.6), (iii) (4,3)D CBCACONHN ($\varepsilon = 6.4$; $^{13}C^{\alpha}$ correlations in basic spectra: 100% yield; S/N: 31.1–72.3; $^{13}C^{\beta}$ correlations in basic spectra: 100% yield; S/N: 23.8–81.1) and (4,3)D CBCA,CONHN ($\varepsilon = 6.4$; intraresidue $^{13}C^{\alpha}$ correlations in basic spectra: 100% yield; S/N: 3.7–23.9; intraresidue $^{13}C^{\beta}$ correlations in basic spectra: 99% yield; S/N: 2.7–9.7). (B) For TT212 we obtained: (5,3)D HACACONHN ($\varepsilon = 25$; 100% yield; S/N for peaks in basic spectra: 3.0–44.6; in first order central peak spectra: 2.5–34.4) and (5,3)D HACA,CONHN ($\varepsilon = 25$; intraresidue correlations: 96% yield; S/N for peaks in basic spectra: 1.5–14.0; 93% in first order central peak spectra: 1.5–14.7). (S/N ratios not reported for other central peak spectra are larger than those of the first order central peaks.)

When using (5,2)D HACACONHN/HACA, CONHN (Figure 3) or (5,3)D HACACONHN and HACA, CONHN (Figure 4), the sequential assignment is based on the three chemical shifts $\Omega(^{13}C')$, $\Omega(^{13}C^{\alpha})$ and $\Omega(^{1}H^{\alpha})$. The use of (4,3)D CBCACONHN/(4,3)D CBCA,CONHN (Figure 5) corresponds to having two 4D experiments in which the number of correlations is increased by a $^{13}C^{\beta}$-$^{13}C^{\alpha}$ relay step. Hence, the (4,3)D experiments likewise provide assignments based on three chemical shifts, i.e., $\Omega(^{13}C')$, $\Omega(^{13}C^{\alpha})$ and $\Omega(^{13}C^{\beta})$. Note, however, that $\Omega(^{13}C^{\alpha})$ and $\Omega(^{13}C^{\beta})$ of a given residue are not directly correlated. Figures 3–5 show that the exhaustive sampling of linear combinations of chemical shifts yields an extended set of sequential connectivities when compared with conventional FT NMR. For example, in (5,3)D HACACONHN/HACA,CONHN seven peaks located at $\Omega_0(^{13}C')\pm\Omega_1(^{13}C^{\alpha})\pm\Omega_2(^{1}H^{\alpha})$ (spectra B1 to B4 in Figure 4), $\Omega_0(^{13}C')\pm\Omega_1(^{13}C^{\alpha})$ (spectra B5 and B6 in Figure 4) and $\Omega_1(^{13}C')$ (spectrum B7 in Figure 4) serve as sequential matching constraints. Recording of 3D HA(CACO)NHN, 3D (HA)CA(CO)NHN and 3D (HACA)CONHN spectra in conjunction with their intraresidue counterparts would yield only 3 constrains, which are devoid of direct correlations between the shifts of $^{13}C'$, $^{13}C^{\alpha}$ and $^{1}H^{\alpha}$ (as provided by the (5,3)D GFT NMR experiment).

Furthermore, the accuracy of chemical shift measurements in constant time GFT NMR experiments scales with $1/(\sqrt{n})$, where n is the number of linear combinations contributing to the determination of a shift (assuming, for simplicity, that the same maximal evolution times have been chosen; Kim and Szyperski, 2003). The increased accuracy of the measurement is documented by comparing the shifts of the same nuclei measured in intra- and interresidue GFT data. Tables 1 to 3 afford a detailed analysis of the shift measurements associated with sequential connectivities shown, respectively, in Figures 3 to 5. These tables provide both the measured linear combinations of shifts and the single-quantum shifts obtained from a linear least-squares fit. The experimental errors for the measurement of the individual linear combinations of the chemical shifts were estimated as described in Kim and Szyperski (2003). The comparison of shifts for the same nucleus as obtained from two different GFT NMR spectra shows that the accuracy is indeed high: the shift differences in Tables 1 to 3 (underlined values; see also Table S1 in the Supplementary Material with the shift analysis corresponding to Figure S2) are smaller than 0.081 ppm for all cases in (5,3)D and (5,2)D GFT NMR spectra, and smaller than 0.154 ppm in the (4,3)D spectra.

Automated resonance assignment (e.g., Szyperski et al., 1998; Moseley et al., 2002) for high-throughput structure determination in structural genomics (Montelione et al., 2000) may profit from employment of GFT NMR in either of the two ways described in the following. First, peak lists of GFT NMR spectra may be used directly to establish sequential connectivities. Then, the extended set of connectivities (see Figures 3–5) corresponding to the matching of $2^m - 1$ *linear combinations* of shifts is redundant and contains ND information. Notably, automated resonance assignment protocols are rather sensitive to the lack of even a smaller number of sequential connectivities. Hence, one can expect to establish more reliable strategies when compared to the use of conventional spectroscopy, also for smaller proteins with molecular weights around 10 kDa. Alternatively, the GFT NMR peak lists can be used to calculate ND peak lists containing accurate single-quantum shifts. Subsequently, sequential connectivities are established based on matching of single-quantum shifts. Due to the increased accuracy of the GFT shift measure-

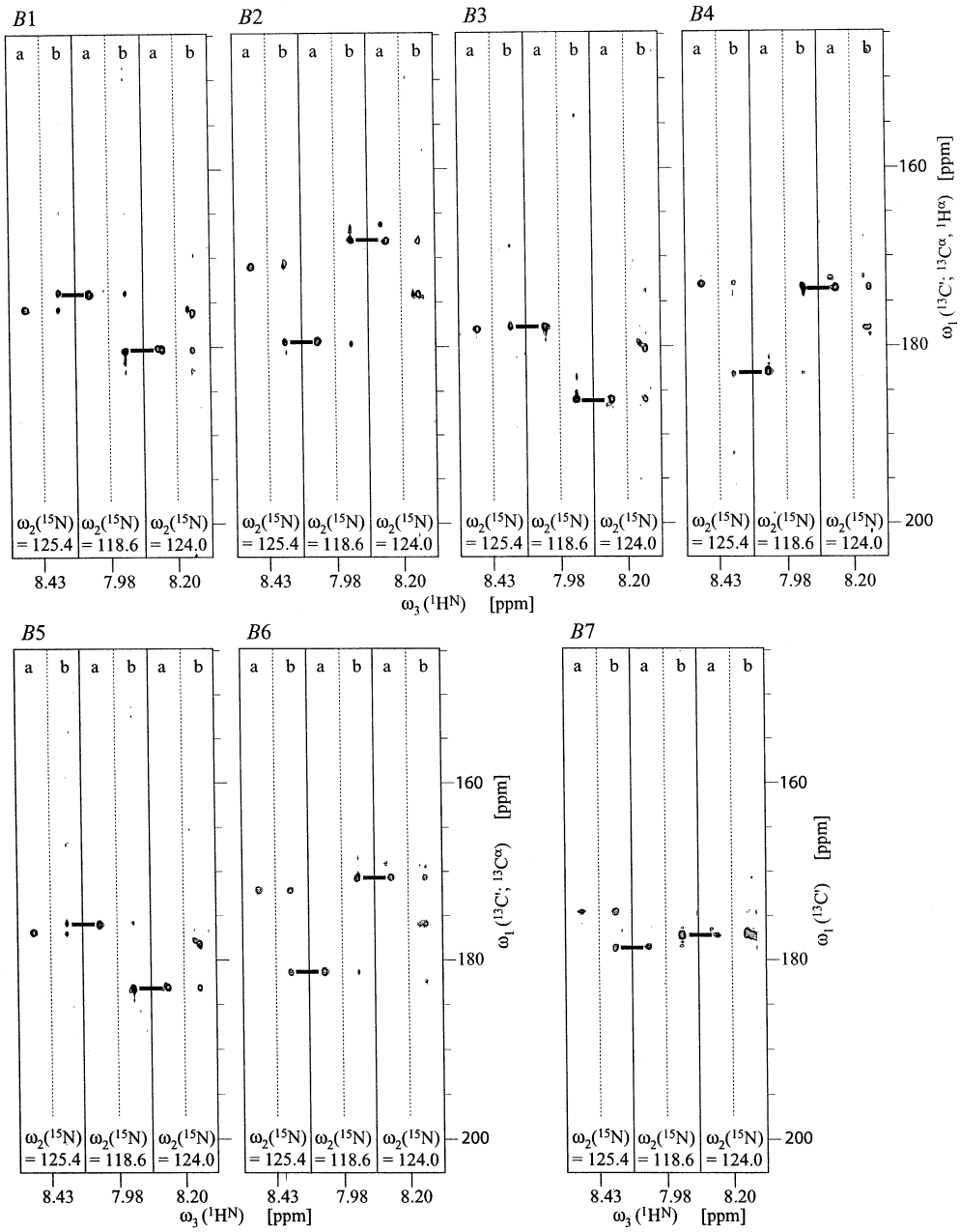

Figure 4. Composite plot of [ω_1,ω_3]-strips taken from (5,3)D HACACONHN (strips labeled with 'a') and (5,3)D HACA,CONHN data (strips labeled with 'b') collected for the 14 kDa NESG consortium target protein TT212 with a total measurement time of 60 h. The 3D data were acquired with 56(t_1) × 24(t_2) × 512(t_3) complex points and $t_{1\,max}(^{13}C'; {}^{13}C^{\alpha}, {}^{1}H^{\alpha}) = 6.2$ ms, $t_{2\,max}(^{15}N) = 16.4$ ms and $t_{3\,max}(^{1}H^{N}) = 73.2$ ms. The first, second and third pair of strips in each block has been taken, respectively, at the ^{15}N chemical shift of Ala 24, Ile 25 and Glu 26 along $\omega_2(^{15}N)$. The strips are centered about the corresponding amide proton shifts detected along $\omega_3(^{1}H^{N})$. The ^{15}N shifts are given at the bottom of each pair of strips, which were taken from basic spectra (*B*1 to *B*4), the first order central peak spectra (*B*5 and *B*6) and the second order central peak spectra (*B*7). The type of linear combination of chemical shifts detected along ω_1 is indicated at the top of the strips: *B*1 [$\Omega_0+\Omega_1+\Omega_2$]; *B*2 [$\Omega_0-\Omega_1+\Omega_2$]; *B*3 [$\Omega_0+\Omega_1-\Omega_2$]; *B*4 [$\Omega_0-\Omega_1-\Omega_2$]; *B*5 [$\Omega_0+\Omega_1$]; *B*6 [$\Omega_0-\Omega_1$]; *B*7 [$\Omega_0$]. Sequential connectivities are indicated by horizontal lines and are established based on the measurement of three chemical shifts, i.e., $\Omega(^{13}C')$, $\Omega(^{13}C^{\alpha})$ and $\Omega(^{1}H^{\alpha})$. The chemical shifts were obtained with high precision (Table 2), since the errors are reduced by the following factors when compared with FT NMR (calculated as described in Kim and Szyperski, 2003). For $\Omega(^{13}C')$: $\sqrt{7} = 2.6$; $\Omega(^{13}C^{\alpha})$: $\sqrt{6} = 2.4$; $\Omega(^{1}H^{\alpha})$: $\sqrt{4} = 2$. ^{1}H and ^{13}C chemical shifts are in ppm relative to 2,2-dimethyl-2-silapentane-5-sulfonate sodium salt (DSS).

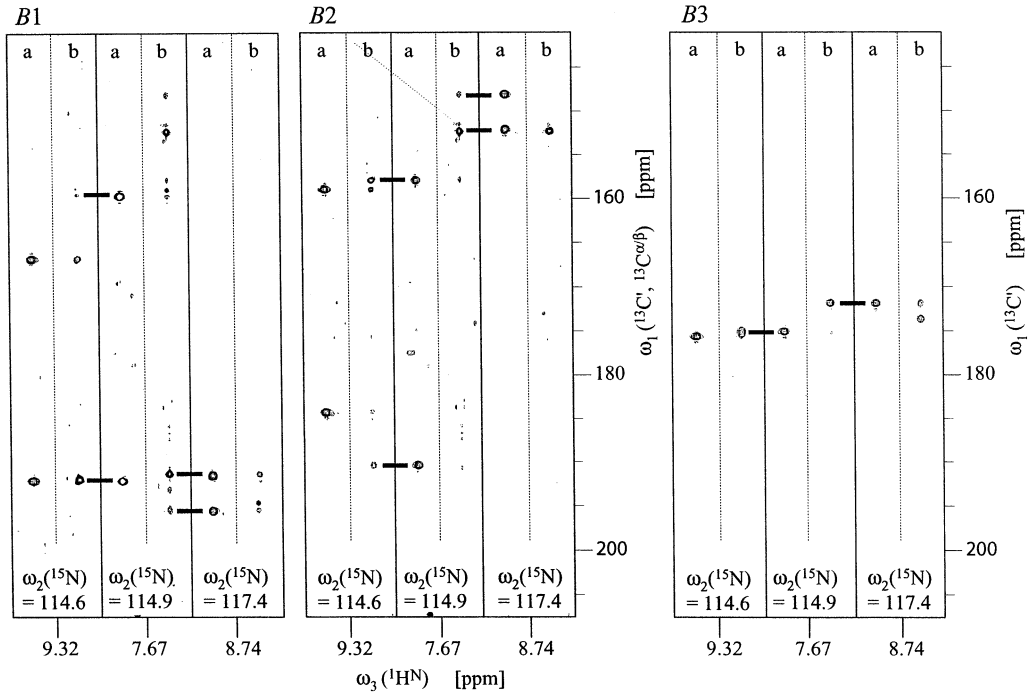

Figure 5. Composite plot of [ω_1, ω_3]-strips taken from (4,3)D CBCACONHN (strips labeled with 'a') and (4,3)D CBCA,CONHN data (strips labeled with 'b') collected for the 8.6 kDa protein ubiquitin with a total measurement time of 11.2 h. The 3D data were acquired with 60(t_1) × 24(t_2) × 512(t_3) complex points and $t_{1\,max}$(^{13}C'; ^{13}C$^{\alpha/\beta}$) = 5.9 ms, $t_{2\,max}$(^{15}N) = 17.2 ms and $t_{3\,max}$(^{1}H^N) = 73.2 ms. The first, second and third pair of strips in each block has been taken, respectively, at the ^{15}N chemical shift of Glu 64, Ser 65 and Thr 66 along ω_2(^{15}N). The strips are centered about the corresponding amide proton shifts detected along ω_3(^{1}H^N). The ^{15}N shifts are given at the bottom of each pair of strips, which were taken from basic spectra (*B*1 and *B*2) and the first order central peak spectra (*B*3). The type of linear combination of chemical shifts detected along ω_1 is indicated at the top of the strips: *B*1 [$\Omega_0 + \Omega_1$]; *B*2 [$\Omega_0 - \Omega$]; *B*3 [Ω_0]. Sequential connectivities are indicated by horizontal lines and are established based on the measurement of three chemical shifts, i.e., Ω(^{13}C'), Ω(^{13}C$^\alpha$) and Ω(^{13}C$^\beta$). [Since the ^{13}C$^{\alpha/\beta}$ carrier was set in between the ^{13}C$^\alpha$ and ^{13}C$^\beta$ chemical shift ranges (Figure 2), one has that peaks at ω_2(^{13}C' + ^{13}C$^\alpha$) and ω_2(^{13}C' + ^{13}C$^\beta$) in B1 appear in a 'reversed order' when compared with B2, which exhibits peaks at ω_2(^{13}C' − ^{13}C$^\alpha$) and ω_2(^{13}C' − ^{13}C$^\beta$).] The chemical shifts were obtained with high precision (Table 3) since the errors are reduced by the following factors when compared with FT NMR (calculated as described in Kim and Szyperski, 2003). For Ω(^{13}C'): $\sqrt{3} = 1.7$; Ω(^{13}C$^\alpha$): $\sqrt{2} = 1.4$; Ω(^{13}C$^\beta$): $\sqrt{2} = 1.4$]. ^{1}H and ^{13}C chemical shifts are in ppm relative to 2,2-dimethyl-2-silapentane-5-sulfonate sodium salt (DSS).

ments, correspondingly reduced matching tolerances (defined as the chemical shift difference between two shift values below which these are considered to be identical) can be employed. For example, the program AUTOASSIGN (Moseley et al., 2002) is routinely executed with matching tolerances of 0.4 ppm for ^{13}C$^{\alpha/\beta}$ shifts, 0.25 ppm for ^{13}C′ shifts and 0.04 ppm for ^{1}H$^\alpha$ shifts measured in indirect dimensions of FT triple resonance NMR spectra (H. Moseley, personal communication). Setting the matching tolerance for analysis of (5,2)D and (5,3)D GFT NMR derived ND peak list to about 2 times the maximal shift difference (Tables 1 to 3), one obtains as a first estimate: ∼0.15 ppm for ^{13}C$^\alpha$ shifts, ∼0.15 ppm for ^{13}C′ shifts and ∼0.02 ppm for ^{1}H$^\alpha$ shifts. Future statistical analysis of several GFT NMR spectra and the use of AUTOASSIGN for GFT NMR data have to reveal the magnitude of the reduction of matching tolerances more accurately, but the estimates presented here clearly show that a significant reduction can be anticipated.

In the context of these considerations, the impact of varying S/N ratios on the accuracy of shift measurements deserves special attention. Depending on the particular protocol that is employed to extract chemical shifts from frequency domain data, the precision of the shift measurement may depend on both the resonance linewidth at half height, $\Delta\nu_{1/2}$, and the signal-to-noise (S/N) ratio (e.g., Cavanagh et al., 1996). For example, if a function describing the expected line shape (e.g., a Lorentzian) is fitted to the experimental data, the chemical shifts are obtained as one of the fitting parameters. Straightforward simulations show that the standard deviation of the shift measurement, σ_m, scales, in a very good approxim-

Table 1. Chemical shifts measured in (5,2)D HACA,CONHN / (5,2)D HACACONHN recorded for ubiquitin (see Figure 3). The underlined values in the lower right represent the differences of single-quantum shifts obtained from (5,2)D HACA,CONHN and (5,2)D HACACONHN.

(A) (5,2)D HACA,CONHN		
Linear combinations of shifts (Glu 64) measured along ω_1 (ppm)		
$\Omega_0(^{15}\mathrm{N}) + \Omega_1(^{13}\mathrm{C}') + \Omega_2(^{13}\mathrm{C}^\alpha) + \Omega_3(^{1}\mathrm{H}^\alpha)$	108.075 ± 0.167	B1
$\Omega_0(^{15}\mathrm{N}) - \Omega_1(^{13}\mathrm{C}') + \Omega_2(^{13}\mathrm{C}^\alpha) + \Omega_3(^{1}\mathrm{H}^\alpha)$	103.697 ± 0.167	B2
$\Omega_0(^{15}\mathrm{N}) + \Omega_1(^{13}\mathrm{C}') - \Omega_2(^{13}\mathrm{C}^\alpha) + \Omega_3(^{1}\mathrm{H}^\alpha)$	97.120 ± 0.167	B3
$\Omega_0(^{15}\mathrm{N}) - \Omega_1(^{13}\mathrm{C}') - \Omega_2(^{13}\mathrm{C}^\alpha) + \Omega_3(^{1}\mathrm{H}^\alpha)$	92.937 ± 0.167	B4
$\Omega_0(^{15}\mathrm{N}) + \Omega_1(^{13}\mathrm{C}') + \Omega_2(^{13}\mathrm{C}^\alpha) - \Omega_3(^{1}\mathrm{H}^\alpha)$	136.303 ± 0.167	B5
$\Omega_0(^{15}\mathrm{N}) - \Omega_1(^{13}\mathrm{C}') + \Omega_2(^{13}\mathrm{C}^\alpha) - \Omega_3(^{1}\mathrm{H}^\alpha)$	131.989 ± 0.167	B6
$\Omega_0(^{15}\mathrm{N}) + \Omega_1(^{13}\mathrm{C}') - \Omega_2(^{13}\mathrm{C}^\alpha) - \Omega_3(^{1}\mathrm{H}^\alpha)$	125.512 ± 0.167	B7
$\Omega_0(^{15}\mathrm{N}) - \Omega_1(^{13}\mathrm{C}') - \Omega_2(^{13}\mathrm{C}^\alpha) - \Omega_3(^{1}\mathrm{H}^\alpha)$	121.182 ± 0.167	B8
$\Omega_0(^{15}\mathrm{N}) + \Omega_1(^{13}\mathrm{C}') + \Omega_2(^{13}\mathrm{C}^\alpha)$	122.043 ± 0.167	B9
$\Omega_0(^{15}\mathrm{N}) - \Omega_1(^{13}\mathrm{C}') + \Omega_2(^{13}\mathrm{C}^\alpha)$	117.721 ± 0.167	B10
$\Omega_0(^{15}\mathrm{N}) + \Omega_1(^{13}\mathrm{C}') - \Omega_2(^{13}\mathrm{C}^\alpha)$	111.432 ± 0.167	B11
$\Omega_0(^{15}\mathrm{N}) - \Omega_1(^{13}\mathrm{C}') - \Omega_2(^{13}\mathrm{C}^\alpha)$	107.122 ± 0.167	B12
$\Omega_0(^{15}\mathrm{N}) + \Omega_1(^{13}\mathrm{C}')$	116.832 ± 0.106	B13
$\Omega_0(^{15}\mathrm{N}) - \Omega_1(^{13}\mathrm{C}')$	112.351 ± 0.106	B14
$\Omega_0(^{15}\mathrm{N})$	114.577 ± 0.078	B15
Single-quantum shifts (ppm)		
$\Omega_0(^{15}\mathrm{N})$	114.593 ± 0.040	
$\Omega_1(^{13}\mathrm{C}')$	175.133 ± 0.017	
$\Omega_2(^{13}\mathrm{C}^\alpha)$	58.427 ± 0.019	
$\Omega_3(^{1}\mathrm{H}^\alpha)$	3.347 ± 0.006	
(B) (5,2)D HACACONHN		
Linear combinations of shifts [$\Omega_0(^{15}\mathrm{N})$ of Ser 65 and of Glu 64 otherwise] measured along ω_1 (ppm)		
$\Omega_0(^{15}\mathrm{N}) + \Omega_1(^{13}\mathrm{C}') + \Omega_2(^{13}\mathrm{C}^\alpha) + \Omega_3(^{1}\mathrm{H}^\alpha)$	108.510 ± 0.167	*B1*
$\Omega_0(^{15}\mathrm{N}) - \Omega_1(^{13}\mathrm{C}') + \Omega_2(^{13}\mathrm{C}^\alpha) + \Omega_3(^{1}\mathrm{H}^\alpha)$	103.758 ± 0.167	*B2*
$\Omega_0(^{15}\mathrm{N}) + \Omega_1(^{13}\mathrm{C}') - \Omega_2(^{13}\mathrm{C}^\alpha) + \Omega_3(^{1}\mathrm{H}^\alpha)$	97.642 ± 0.167	*B3*
$\Omega_0(^{15}\mathrm{N}) - \Omega_1(^{13}\mathrm{C}') - \Omega_2(^{13}\mathrm{C}^\alpha) + \Omega_3(^{1}\mathrm{H}^\alpha)$	92.982 ± 0.167	*B4*
$\Omega_0(^{15}\mathrm{N}) + \Omega_1(^{13}\mathrm{C}') + \Omega_2(^{13}\mathrm{C}^\alpha) - \Omega_3(^{1}\mathrm{H}^\alpha)$	136.891 ± 0.167	*B5*
$\Omega_0(^{15}\mathrm{N}) - \Omega_1(^{13}\mathrm{C}') + \Omega_2(^{13}\mathrm{C}^\alpha) - \Omega_3(^{1}\mathrm{H}^\alpha)$	131.088 ± 0.167	*B6*
$\Omega_0(^{15}\mathrm{N}) + \Omega_1(^{13}\mathrm{C}') - \Omega_2(^{13}\mathrm{C}^\alpha) - \Omega_3(^{1}\mathrm{H}^\alpha)$	125.054 ± 0.167	*B7*
$\Omega_0(^{15}\mathrm{N}) - \Omega_1(^{13}\mathrm{C}') - \Omega_2(^{13}\mathrm{C}^\alpha) - \Omega_3(^{1}\mathrm{H}^\alpha)$	121.270 ± 0.167	*B8*
$\Omega_0(^{15}\mathrm{N}) + \Omega_1(^{13}\mathrm{C}') + \Omega_2(^{13}\mathrm{C}^\alpha)$	122.727 ± 0.167	*B9*
$\Omega_0(^{15}\mathrm{N}) + \Omega_1(^{13}\mathrm{C}') - \Omega_2(^{13}\mathrm{C}^\alpha)$	111.894 ± 0.167	*B10*
$\Omega_0(^{15}\mathrm{N}) - \Omega_1(^{13}\mathrm{C}') + \Omega_2(^{13}\mathrm{C}^\alpha)$	117.984 ± 0.167	*B11*
$\Omega_0(^{15}\mathrm{N}) - \Omega_1(^{13}\mathrm{C}') - \Omega_2(^{13}\mathrm{C}^\alpha)$	107.206 ± 0.167	*B12*
$\Omega_0(^{15}\mathrm{N}) + \Omega_1(^{13}\mathrm{C}')$	116.198 ± 0.106	*B13*
$\Omega_0(^{15}\mathrm{N}) - \Omega_1(^{13}\mathrm{C}')$	112.608 ± 0.106	*B14*
$\Omega_0(^{15}\mathrm{N})$	114.886 ± 0.078	*B15*
Single-quantum shifts (ppm)		
$\Omega_0(^{15}\mathrm{N})$ (Ser 65)	114.913 ± 0.040	
$\Omega_1(^{13}\mathrm{C}')$	175.210 ± 0.017 $\underline{-0.077}$	
$\Omega_2(^{13}\mathrm{C}^\alpha)$	58.440 ± 0.019 $\underline{-0.013}$	
$\Omega_3(^{1}\mathrm{H}^\alpha)$	3.344 ± 0.006 $\underline{+0.003}$	

ation, linearly with the inverse of the S/N ratio for S/N > 2. Provided that identical measurement times are invested, the 2^K peaks in the basic spectra of a GFT NMR experiment, which correspond to a single peak in the parent experiment, exhibit S/N ratios that are reduced by $\sqrt{2^K}$ compared to the parent peak (Kim and Szyperski, 2003). Consequently, σ_m for each of the linear combinations of shifts measured in GFT NMR is increased by about $\sqrt{2^K}$ when compared to σ_m of the chemical shifts measured in the parent experiment. On the other hand, a reduction of σ_m by $\sqrt{2^K}$ is gained in constant time GFT NMR spectroscopy after the least-squares fit yielding single-quantum shifts from an overdetermined system of 2^K equations (Kim and Szyperski, 2003). Hence, in the ideal case of having experimental data that are affected solely by Gaussian white noise and having high digital resolution allowing one to fit (a known) line shape function, the precision of the single-quantum shift measurements obtained from the set of 2^K *basic* GFT spectra or from the conventional NMR spectrum, both acquired with the same measurement time, are quite comparable. Provided that central peaks are derived from heteronuclear steady state magnetization, i.e., from axial magnetization that is discarded in conventional spectroscopy (Szyperski et al., 1996), the chemical shifts additionally encoded in the central peaks are obtained with correspondingly higher precision in GFT NMR. However, the major obstacles for realizing both precise and accurate measurements of chemical shifts in conventional multidimensional NMR spectroscopy by line shape fitting are (i) the poor digitization of indirect dimensions in higher dimensional NMR spectra (see, for example, Figure 7 in Kim and Szyperski, 2003), (ii) the presence of non Gaussian, colored noise (Grage and Akke, 2003) and spectral artefacts, (iii) line shape variations arising from employment of linear prediction of time domain data for resolution enhancement (Cavanagh et al., 1996), (iv) smaller phase errors arising from off-resonance effects of r.f. pulses and (v) peak overlap. As a consequence, even if one would obtain some increase in *precision* through line fitting this would not necessarily warrant increased *accuracy*. Hence, multidimensional correlation spectra are quite generally analyzed by identifying the peak maxima ('peak picking'), that is, above a threshold ensuring secure identification peak intensities are not considered for the measurement of chemical shifts, and alternative approaches, such as GFT NMR, are required for accurate measurement of chemical shifts registered in indirect dimensions of multidimensional spectroscopy.

Table 2. Chemical shifts measured in (5,3)D HACA,CONHN/(5,3)D HACACONHN recorded for TT212 (see Figure 4). The underlined values in the lower right represent the differences of single-quantum shifts obtained from (5,3)D HACA,CONHN and (5,3)D HACACONHN.

(A) (5,3)D HACA,CONHN		
Linear combinations of shifts (Ile 25) measured along ω_1 (ppm)		
$\Omega_0(^{13}C') + \Omega_1(^{13}C^\alpha) + \Omega_2(^1H^\alpha)$	180.354 ± 0.067	*B*1
$\Omega_0(^{13}C') - \Omega_1(^{13}C^\alpha) + \Omega_2(^1H^\alpha)$	167.916 ± 0.067	*B*2
$\Omega_0(^{13}C') + \Omega_1(^{13}C^\alpha) - \Omega_2(^1H^\alpha)$	185.688 ± 0.067	*B*3
$\Omega_0(^{13}C') - \Omega_1(^{13}C^\alpha) - \Omega_2(^1H^\alpha)$	173.824 ± 0.067	*B*4
$\Omega_0(^{13}C') + \Omega_1(^{13}C^\alpha)$	183.169 ± 0.067	*B*5
$\Omega_0(^{13}C') - \Omega_1(^{13}C^\alpha)$	170.699 ± 0.067	*B*6
$\Omega_0(^{13}C')$	177.140 ± 0.045	*B*7
Single-quantum shifts (ppm)		
$\Omega_0(^{13}C')$	176.970 ± 0.024	
$\Omega_1(^{13}C^\alpha)$	62.389 ± 0.027	
$\Omega_2(^1H^\alpha)$	4.073 ± 0.009	
(B) (5,3)D HACACONHN		
Linear combinations of shifts (Ile 25) measured along ω_1 (ppm)		
$\Omega_0(^{13}C') + \Omega_1(^{13}C^\alpha) + \Omega_2(^1H^\alpha)$	180.223 ± 0.067	*B*1
$\Omega_0(^{13}C') - \Omega_1(^{13}C^\alpha) + \Omega_2(^1H^\alpha)$	168.256 ± 0.067	*B*2
$\Omega_0(^{13}C') + \Omega_1(^{13}C^\alpha) - \Omega_2(^1H^\alpha)$	185.907 ± 0.067	*B*3
$\Omega_0(^{13}C') - \Omega_1(^{13}C^\alpha) - \Omega_2(^1H^\alpha)$	173.603 ± 0.067	*B*4
$\Omega_0(^{13}C') + \Omega_1(^{13}C^\alpha)$	183.052 ± 0.067	*B*5
$\Omega_0(^{13}C') - \Omega_1(^{13}C^\alpha)$	170.933 ± 0.067	*B*6
$\Omega_0(^{13}C')$	177.075 ± 0.045	*B*7
Single-quantum shifts (ppm)		
$\Omega_0(^{13}C')$	177.007 ± 0.024	$\underline{-0.037}$
$\Omega_1(^{13}C^\alpha)$	62.325 ± 0.027	$\underline{+0.064}$
$\Omega_2(^1H^\alpha)$	4.087 ± 0.009	$\underline{-0.014}$

In order to assess errors of shift measurements and their propagation in GFT NMR, we have thus previously (Kim and Szyperski, 2003) adopted a statistical model in which the error for the identification of peak maximum is associated with a Gaussian distribution and the line width at half height, $\Delta\nu_{1/2}$, represents the corresponding 99.7% confidence interval (i.e., $\Delta\nu_{1/2} = 6\sigma$). Such a Gaussian distribution has been chosen in order to consider the other sources for erroneous peak picking given above. Moreover, the statistical model focusses on the line widths as the primary determinants for the accuracy, since uncharacterized error sources and poor digitization usually impede accurate line fitting. The approach is conservative in the sense that it is only requested that the peak maxima are identified with 99.7% confidence within

Table 3. Chemical shifts measured in (4,3)D CB,CACONHN/(4,3)D CBCACONHN recorded for ubiquitin (see Figure 5). The underlined values in the lower right represent the differences of single-quantum shifts obtained from (4,3)D CB,CACONHN and (4,3)D CBCACONHN.

(A) (4,3)D CBCA,CONHN		
Linear combinations of shifts (Ser 65) measured along ω_1 (ppm)		
$\Omega_0(^{13}C') + \Omega_1(^{13}C^{\alpha})$	191.359 ± 0.067	*B*1
$\Omega_0(^{13}C') + \Omega_1(^{13}C^{\beta})$	195.451 ± 0.067	*B*1
$\Omega_0(^{13}C') - \Omega_1(^{13}C^{\alpha})$	152.401 ± 0.067	*B*2
$\Omega_0(^{13}C') - \Omega_1(^{13}C^{\beta})$	148.249 ± 0.067	*B*2
$\Omega_0(^{13}C')$	171.848 ± 0.045	*B*3
Single-quantum shifts (ppm)		
$\Omega_0(^{13}C')$	171.862 ± 0.027	
$\Omega_1(^{13}C^{\alpha})$	60.789 ± 0.047	
$\Omega_1(^{13}C^{\beta})$	64.911 ± 0.047	
(B) (4,3)D CBCACONHN		
Linear combinations of shifts (Ser 65) measured along ω_1 (ppm)		
$\Omega_0(^{13}C') + \Omega_1(^{13}C^{\alpha})$	191.533 ± 0.067	*B*1
$\Omega_0(^{13}C') + \Omega_1(^{13}C^{\beta})$	195.530 ± 0.067	*B*1
$\Omega_0(^{13}C') - \Omega_1(^{13}C^{\alpha})$	152.267 ± 0.067	*B*2
$\Omega_0(^{13}C') - \Omega_1(^{13}C^{\beta})$	148.225 ± 0.067	*B*2
$\Omega_0(^{13}C')$	171.887 ± 0.045	*B*3
Single-quantum shifts (ppm)		
$\Omega_0(^{13}C')$	171.888 ± 0.027	$\underline{-0.026}$
$\Omega_1(^{13}C^{\alpha})$	60.943 ± 0.047	$\underline{-0.154}$
$\Omega_1(^{13}C^{\beta})$	64.962 ± 0.047	$\underline{-0.051}$

$\Delta\nu_{1/2}$. (Note, that even at very moderate S/N ratios around 2, the probability that white Gaussian spectrometer noise shifts the peak maximum outside of the range of $\Delta\nu_{1/2}$ is, for practical purposes, negligible.) Importantly, spectral analysis is often hampered by artefacts to a degree that is at least comparable to the limitations arising from noise. It is thus of great advantage that the peaks in the $2^{K+1} - 1$ spectra constituting a GFT NMR experiment exhibit distinct symmetries resulting from the exhaustive sampling of linear combinations of chemical shifts. The likelihood that GFT NMR peak pattern are generated by chance as a result of noise fluctuations and/or spectral artefacts is negligible for $K > 1$. Hence, the symmetry properties allow one to identify peaks with intensities that are closer to the noise level when compared with the analysis of conventional data. Within the above described procedure to measure chemical shifts by 'peak picking' and the correspondingly chosen statistical model (Kim and Szyperski, 2003), the accuracy of shift measurements using constant time GFT NMR experiments is largely independent of transverse relaxation rates (which solely determine the peak intensity) and thus of the molecular weight. This robustness ensures that the conclusions with respect to the impact of GFT NMR for automated resonance assignment, or NMR-based structural biology in general, are rather generally valid for a broad range of molecular weights.

A special comment relates to the detection of sequential peaks in the experiments providing the intraresidue connectivities. In principle, one may 'filter out' the sequential connectivities (e.g., Brutscher, 2002). However, we prefer not to eliminate sequential peaks, since (i) such filtering compromises on the sensitivity, (ii) the sequential peaks can be readily identified in the sequential congener, and (iii) the sequential peaks in the intraresidue experiment can be used to accurately adjust the calibration of the two GFT NMR spectra used in conjunction. For automated assignment protocols, the procedure alluded to in point (iii) is of outstanding value to reduce matching tolerances and is thus routinely employed. At highest magnetic fields (900 MHz ^{1}H resonance frequency), it might be advantageous to design GFT experiments providing the sequential connectivities in a manner suggested by Meissner and Sørensen (2001).

In view of the introduction of cryogenic probes, which reduce NMR measurement times by a factor of 10 or more (e.g., Monleon et al., 2002), GFT NMR experiments providing 4D and 5D NMR spectral information are highly attractive also for larger systems. For example, (5,2)D HACACONHN/HACA,CONHN and (4,3)D CBCACONHN/CBCA,CONHN were acquired in only 10.6 and 11.2 h, respectively, for an 8.6 kDa protein and it can thus be expected that similarly short measurement times are feasible for medium-sized protein up to about 20 kDa when using cryogenic probes. In fact, the (5,3)D data sets of 14 kDa TT212 (Figure 4) were acquired in about 60 h, so that the same data could have been recorded within a few hours with a cryogenic probe. Apart from sensitivity, spectral resolution is critical for employment of multidimensional NMR. At high magnetic fields, (4,3)D and (5,3)D ^{15}N-resolved GFT NMR experiments are well suited to approach large proteins, at least to the extent the conventional ^{15}N-resolved 3D congeners are currently used. For the (5,2)D experiments, one needs to consider that peak dispersion increases linearly from third order (2D [^{15}N,^{1}H]-HSQC), to second order to first order and to basic spectra (see Figure 6 in Kim and Szyperski, 2003). Moreover, future research needs to show how effectively computer supported

'bottom-up' identification of chemical shift multiplets restores the 5D dispersion (Kim and Szyperski, 2003). Certainly, the dispersion of the 2D [^{15}N,^{1}H]-HSQC provides a good initial indication with respect to the degree of overlap that needs to be resolved during the 'bottom-up' assignment. At 900 MHz ^{1}H resonance frequency, 20-25 kDa proteins often exhibit rather well resolved 2D [^{15}N,^{1}H]-TROSY (Pervushin et al., 1997) spectra (e.g., Liu et al., 2003), and we thus expect that proteins up to a least 20 kDa might well be approached using (5,2)D GFT-TROSY NMR at such highest field strengths.

Finally, future research will show to which extent the acquisition speed of GFT NMR can be further increased by combination with recently introduced 2D/3D single scan acquisition (Frydman et al., 2002) or Hadamard-type sampling schemes (Kupce and Freeman, 1993; 2003). Moreover, it is conceivable that the 'sampling demand' of GFT NMR can be further reduced by (i) non-linear sampling (e.g., Schmieder et al., 1994), (ii) the employment of the filter diagonalization approach for data processing (Wall and Neuhauser, 1995, Hu et al., 1998), or (iii) the use of 'three-way decomposition' (Gutmanas et al. 2002).

Acknowledgements

This work was supported by the *National Science Foundation (*MCB 0075773) and the *National Institutes of Health* (P50 GM62413-01). We thank Drs C. Arrowsmith and A. Yee (University of Toronto) for providing the TT212 sample, Drs M. Kennedy and J. Cort (Pacific Northwest National Laboratories) for providing the ubiquitin sample, Mr Yang Shen for providing the chemical shifts of TT212, and Drs Montelione and Moseley (Rutgers University) for helpful discussions. Two figures and a table are available as supplementary material from the corresponding author. (i) Figure S1 with the pulse sequence used for (4,3)D CBCACONHN data acquisition, (ii) Figure S2 with a composite of plot of strips taken from the (5,3)D spectra acquired for ubiquitin, (iii) Table S1 with the chemical shifts of correlations shown in Figure S2.

References

Astrof, N.S., Lyon, C.E. and Griffin, R.G. (2001) *J. Magn. Reson.*, **152**, 303–307.

Bax, A. (2003) *Protein Sci.*, **12**, 1–16.

Bersch, B., Rossy, E., Coves, J. and Brutscher, B. (2003) *J. Biomol. NMR*, **27**, 57–67.

Bodenhausen, G. and Ernst, R.R. (1982) *J. Am. Chem. Soc.*, **104**, 1304–1309.

Boelens, R., Burgering, M., Fogh, R.H. and Kaptein, R. (1994) *J. Biomol. NMR*, **4**, 201–213.

Brutscher, B. (2002) *J. Magn. Reson.*, **156**, 155–159.

Brutscher, B., Cordier, F., Simorre, J.-P., Caffrey, M.S. and Marion, D. (1995a) *J. Biomol. NMR*, **5**, 202–206.

Brutscher, B., Morelle, N., Cordier, F. and Marion, D. (1995b) *J. Magn. Reson.*, **B109**, 238–242.

Brutscher, B., Simorre, J.-P., Caffrey and Marion, D. (1994) *J. Magn. Reson.*, **B105**, 77–82.

Brutscher, B., Skrynnikov, N.R., Bremi, T., Bruschweiler, R. and Ernst, R.R. (1998) *J. Magn. Reson.*, **130**, 346–351.

Cavanagh, J., Fairbrother, W.J., Palmer III, A.G. and Skelton, N.J. (1996) *Protein NMR Spectroscopy*, Wiley, New York.

Ding, K. and Gronenborn, A.M. (2002) *J. Magn. Reson.*, **156**, 262–268.

Frydman, L., Scherf, T. and Lupulescu, A. (2002) *Proc. Natl. Acad. Sci. USA*, **99**, 15858–15862.

Grage, H. and Akke, M. (2003) *J. Magn. Reson.*, **162**, 176–188.

Grzesiek, S. and Bax, A. (1992) *J. Am. Chem. Soc*, **114**, 6291–6293.

Gutmanas, A., Jarvoll, P., Orekhov, V.Y. and Billeter, M. (2002) *J. Biomol. NMR*, **24**, 191–201.

Hu, H., Van, Q.N., Mandelshtam, V.A. and Shaka, A.J. (1998) *J. Magn. Reson.*, **134**, 76–87.

Kay, L.E., Keifer, P. and Saarinen, T. (1992) *J. Am. Chem. Soc.*, **114**, 10663–10665.

Kim, S. and Szyperski, T. (2003) *J. Am. Chem. Soc.*, **125**, 1385–1393.

Kozminski, W. and Zhukov, I. (2003) *J. Biomol. NMR*, **26**, 157–166.

Kupce, E. and Freeman, R. (1993) *J. Magn. Reson. Ser A*, **105**, 310–315.

Kupce, E. and Freeman, R. (2003) *J. Biomol. NMR*, **25**, 349–354.

Liu, G., Mills, J.L., Hess, T.A., Kim, S., Skalicky, J.J., Sukumaran, D.K., Kupce, E., Skerra, A. and Szyperski, T. (2003) *J. Biomol. NMR*, **27**, 187–188.

Löhr, F. and Rüterjans, H. (1995) *J. Biomol. NMR*, **6**, 189–197.

Luca, S. and Baldus, M. (2002) *J. Magn. Reson.*, **159**, 243–249.

Meissner, A. and Sørensen, O.W. (2001) *J. Magn. Reson.*, **150**, 100–104.

Monleon, D., Colson, K., Moseley, H.N.B., Anklin, C., Oswald, R., Szyperski, T. and Montelione, G.T. (2002) *J. Struct. Funct. Genomics*, **2**, 93–101.

Montelione, G.T., Zheng, D., Huang, Y., Gunsalus, C. and Szyperski, T. (2000) *Nat. Struct. Biol.*, **7**, 982–984.

Moseley, H.N.M., Tejero, R., Zimmerman, D.E., Celda, B., Nilsson, B. and Montelione, G.T. (2002) *Meth. Enzymol.*, **339**, 91–108.

Pervushin, K., Riek, R., Wider, G. and Wüthrich, K. (1997) *Proc. Natl. Acad. Sci. USA*, **99**, 8009–8014.

Reif, B., Hennig, M. and Griesinger, C. (1997) *Science*, **276**, 1230–1233.

Rexroth, A., Schmidt, P., Szalma, S., Geppert, T., Schwalbe, H. and Griesinger, C. (1995) *J. Am. Chem. Soc.*, **117**, 10389–10391.

Schmieder, P., Stern, A.S., Wagner, G. and Hoch, J.C. (1994) *J. Biomol. NMR,* **4**, 483–490.

Simorre, J.-P., Brutscher, B., Caffrey, M.S. and Marion, D. (1994) *J. Biomol. NMR*, **4**, 325–333.

Sklenar, V., Dieckmann, T., Butcher, S.E. and Feigon, J. (1998) *J. Magn. Reson.*, **130**, 119–124.

Szyperski, T., Banecki, B., Braun, D. and Glaser, R.W. (1998) *J. Biomol. NMR*, **11**, 387–405.

Szyperski, T., Braun, D., Banecki, B. and Wüthrich, K. (1996) *J. Am. Chem. Soc.*, **118**, 8146–8147.
Szyperski, T., Braun, D., Fernandez, C., Bartels, C. and Wüthrich, K. (1995) *J. Magn. Reson.*, **B108**, 197–203.
Szyperski, T., Pellecchia, M. and Wüthrich, K. (1994) *J. Magn. Reson.*, **B 105**, 188–191.
Szyperski, T., Wider, G., Bushweller, J.H. and Wüthrich, K. (1993a) *J. Biomol. NMR*, **3**, 127–132.
Szyperski, T., Wider, G., Bushweller, J.H. and Wüthrich, K. (1993b) *J. Am. Chem. Soc.*, **115**, 9307–9308.
Szyperski, T., Yeh, D.C., Sukumaran, D.K., Moseley, H.N.B. and Montelione, G.T. (2002) *Proc. Natl. Acad. Sci. USA*, **99**, 8009–8014.
Xia, Y., Arrowsmith, C. and Szyperski, T. (2002) *J. Biomol. NMR*, **24**, 41–50.
Wall, M.R. and Neuhauser, D. (1995) *J. Chem. Phys.*, **112**, 8011–8022.
Zweckstetter, M. and Bax, A. (2001) *J. Am. Chem. Soc.*, **123**, 9490–9491.